Impact of Inverter-Interfaced Renewable Energy Generators on Distance Protection and an Improved Scheme

Yu Fang, Ke Jia, *Member, IEEE*, Zhe Yang, Yanbin Li, and Tianshu Bi, *Senior Member, IEEE*

***Abstract*—With different structures and control strategies, inverter-interfaced renewable energy generators (IIREGs) have different fault characteristics from synchronous generators. This makes the conventional distance protection used in networks with synchronous generators not applicable for transmission lines emanating from IIREGs. Therefore, supported by the fault current analysis, operating performances of distance relays on both sides of the transmission line are unveiled. It reveals the problem that the conventional distance relay on the IIREG side has a high risk of malfunction or refusing to operate. To cope with this adaptability problem, an improved scheme based on time delay and zero-sequence impedance is proposed in this paper. To validate the operating performances of the scheme, a detailed IIREG model is built in a real-time digital simulator, and simulation tests are carried out. Apart from these, a field short-circuit test is performed in a real wind power plant to examine the practical feasibility of the proposed scheme. Both the simulation results and the field test confirm the problem of the conventional distance protection and verify the reliability of the improved scheme.**

***Index Terms*—Distance protection, fault current analysis, inverter-interfaced renewable power generator, outgoing transmission line, relay scheme.**

I. Introduction

As CLEAN and renewable energy power, wind and photovoltaic can significantly reduce the dependence of electricity on fossil fuels and carbon emissions from electric power plants [1]–[3]. Benefiting from the improvement of power electronic technology, centralized large-scale wind farms and photovoltaic plants are being worldwide deployed [4]. Large-scale renewable energy sources are usually connected to the ac system through high-voltage outgoing transmission lines so that enormous capacity of power can be transported from the windy or light-rich regions to the load centers [5]. With the expansion of the capacity of renewable energy sources [6], [7], the requirements for the reliability and quickness of the protection in the case of a transmission line failure are more stringent. For the conventional ac grid, the operation condition of the power system has a little effect on the protection range and sensitivity of the distance protection [8]; hence, distance protection is widely utilized in a complex power grid with high-voltage levels. However, renewable energy sources are usually connected to the ac grid through converters, whose fault characteristics are influenced by control strategies [9], [10]. Due to the different characteristics between renewable energy generators and synchronous generators [11], [12], the conventional protection based on fault characteristics of synchronous generators cannot meet the demand of the renewable energy system [13]. Therefore, it is necessary to study the adaptability of distance protection with renewable energy generators.

There have been some research achievements on the impact of large-scale renewable energy generators on distance protection so far. For outgoing transmission lines of type-III wind farms (WFs), effects of the rotor-speed-related frequency electrical quantities and the equivalent sequence impedances on distance protection were analyzed in [14] and [15]. As described in [16]–[18], research studies on the adaptive setting of distance relays were often based on the characteristics of doubly fed induction generators. Conclusions of the above research studies were only applicable to the transmission lines connected to type-III WFs.

For inverter-interfaced renewable energy generators (IIREGs) that include type-IV WFs and photovoltaic plants, with consideration of different control strategies, the performance of distance protection on the renewable energy source side was analyzed with substantial simulation results [19]. In [20], an adaptive relay setting principle for distance protection was proposed. By obtaining voltages and flows of all parts of the system, the trip boundary of distance relay was reset adaptively. In addition, based on the information of bus voltage, current, and the number of wind turbine units, a method to estimate the error impedance of distance protection was put forward in [21]. New boundaries were set according to the error impedance. Both of these two adaptive schemes required high-performance microprocessors

Manuscript received April 2, 2018; revised June 29, 2018 and August 8, 2018; accepted September 7, 2018. Date of publication October 24, 2018; date of current version April 30, 2019. This work was supported in part by the National Key Research and Development Program of China under Grant 2018YFB0904104, in part by the National Natural Science Foundation of China under Grant 51725702 and Grant 51407067, and in part by the Science and Technology Guide Project of State Grid Corporation (Research on New Protection Control Technology for AC Side of Flexible DC System). *(Corresponding author: Ke Jia.)*

Y. Fang, K. Jia, Z. Yang, and T. Bi are with the State Key Laboratory of Alternative Electrical Power System with Renewable Energy Sources, North China Electric Power University, Beijing 102206, China (e-mail: yuk.fong@outlook.com; ke.jia@ncepu.edu.cn; mr.yangzhe@outlook.com; tsbi@ncepu.edu.cn).

Y. Li is with the North China Branch of State Grid Corporation of China, Beijing 100053, China (e-mail: lyb_zjpj@126.com).

Color versions of one or more of the figures in this paper are available online at http://ieeexplore.ieee.org.

Digital Object Identifier 10.1109/TIE.2018.2873521

0278-0046 © 2018 IEEE. Personal use is permitted, but republication/redistribution requires IEEE permission.
See http://www.ieee.org/publications_standards/publications/rights/index.html for more information.

Authorized licensed use limited to: Washington State University. Downloaded on December 10,2023 at 05:24:04 UTC from IEEE Xplore. Restrictions apply.

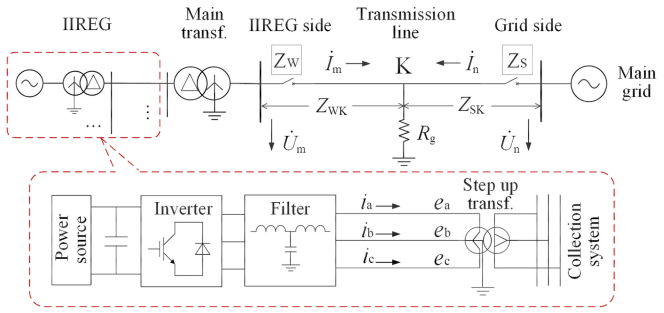

Fig. 1. Topology of a transmission system with an inverter-interfaced renewable energy generator.

and reliable communication techniques with high penetration level of WFs. However, these requirements might not be met in some power grids. In [22], a novel scheme based on an advanced line-impedance formula was proposed to recognize line-to-line-to-ground (LLG) faults effectively. In the formula, the zero-sequence components are adopted, and the remote infeed and the fault resistance had a little effect on the fault impedance. Nevertheless, due to the lack of the zero-sequence component, this high-performance scheme cannot be directly adopted to line-to-line (LL) faults. As an ideal primary protection widely used in conventional transmission lines, differential protection was analyzed in detail in terms of the operating performance for the outgoing transmission lines emanating from the IIREG in [23]. The literature pointed out that due to the deviation of the phase angle of the short-circuit currents on the two terminals caused by control actions after internal faults, the conventional differential protection might suffer from low sensitivity when large-scale WFs are integrated [24].

At present, the outgoing transmission line is often equipped with differential protection, distance-based protection [25], and zero-sequence overcurrent protection on the IIREG side. The distance protection is sometimes blocked due to the unique fault characteristics of large-scale IIREGs. With the increased penetration of IIREGs, given that the sensitivity of differential protection is not sufficient and the protection may even fail to operate for internal faults as described in [23], it is necessary to further analyze the operating performance of distance relays and propose an improved scheme, which can minimize the side impacts of the fault characteristics of IIREGs.

In this paper, for the transmission line emanating from IIREGs, the fault current expression is deduced, and the operating performance of distance protection is analyzed. To solve the defects that the IIREG-side distance protection would malfunction or refuse to operate, an improved scheme is put forward. Simulation results and the field test validate the wide applicability and practical feasibility of the proposed scheme, respectively.

II. Failure Characteristics Analysis of IIREGs

The typical IIREG depicted in Fig. 1 is composed of a power source, an inverter, an *LCL* filter, and a step-up transformer that boosts the voltage up to the medium level.

When an asymmetric fault occurs, in order to meet the control objectives that usually contain suppressing negative-sequence current and suppressing active or reactive power oscillations [26], [27], the IIREG regulates positive- and negative-sequence current references, respectively, by adopting a *dq* synchronous rotating frame [9]. Such current references can be calculated as [28]

$$\begin{bmatrix} i_d^{+*} \\ i_q^{+*} \\ i_d^{-*} \\ i_q^{-*} \end{bmatrix} = \frac{2}{3} \begin{bmatrix} e_d^+ & e_q^+ \\ e_q^+ & -e_d^+ \\ -Ke_d^- & Ke_q^- \\ -Ke_q^- & -Ke_d^- \end{bmatrix} \begin{bmatrix} P^* \\ \bar{M} \\ Q^* \\ \bar{N} \end{bmatrix} \tag{1}$$

where e_d^+, e_q^+, e_d^-, and e_q^- are the terminal voltages of the IIREG under the double synchronous rotating frame. P^* and Q^* are the target active and reactive power commands, respectively. $M = (e_d^+)^2 + (e_q^+)^2 - K[(e_d^-)^2 + (e_q^-)^2]$, $N = (e_d^+)^2 + (e_q^+)^2 + K[(e_d^-)^2 + (e_q^-)^2]$, and K is an integer variable, which equals 0, 1, or -1 for suppressing negative-sequence current, active power, or reactive power oscillations, respectively, during the fault-ride-through (FRT) period.

Take the control strategy, which aims at balancing three-phase ac current for instance. For this control objective, the short-circuit current merely contains the component of the positive-sequence part. Therefore, it can be expressed as

$$i_\phi = \frac{2}{3}\sqrt{\frac{(P^*)^2 + (Q^*)^2}{(e_d^+)^2 + (e_q^+)^2}}\cos(\omega t + \theta_0 + \varphi + \theta_\phi) \tag{2}$$

where the subscript ϕ represents phase A, B, or C. ω is the power-frequency electrical angular velocity. θ_0 is the angle between the d^+-axis and the α-axis when faults occur. $\theta_a = 0°$, $\theta_b = -120°$, and $\theta_c = 120°$; $\varphi = \arctan(e_q^+ P^* - e_d^+ Q^*)/(e_d^+ P^* + e_q^+ Q^*)$.

It is known from (2) that the amplitude of the short-circuit current is dictated by the voltage level, target active, and reactive power commands during FRT, while the inception angle is determined based on the time of fault as well.

Considering a serious voltage dip after the failure, the three-phase short-circuit current amplitude will exceed the maximum allowable value. To protect the inverter from destruction, the *d*- and *q*-axis components of the current references are usually passed through a saturation block element. Once the maximum value of the three-phase currents, denoted by $i_{\max}$, exceeds $i_{\lim}$, the positive-sequence current references are reset to $i_d^{+*} \times (i_{\lim}/i_{\max})$ and $i_q^{+*} \times (i_{\lim}/i_{\max})$. Under this circumstance, the short-circuit current is limited, and the initial phase angle is not changed.

When other control objectives, such as suppressing active power oscillations, suppressing reactive power oscillations, and taking the flexible and semiflexible power control strategies described in [29], are adopted, a large negative-sequence component will appear in the three-phase currents after faults. Except this, the other characteristics of the short-circuit current are basically unchanged, that is, the amplitude of the short-circuit current is still limited, and the phase angle is still controlled. Since the negative-sequence impedance of the outgoing

Authorized licensed use limited to: Washington State University. Downloaded on December 10,2023 at 05:24:04 UTC from IEEE Xplore. Restrictions apply.

transmission line is equal to the positive-sequence one, the value of the negative-sequence current does not substantially affect the performance of the distance protection. For these factors, the control objective of suppressing the negative-sequence current is taken as an example for analysis.

To sum up, under the typical low-voltage ride-through control strategies, the amplitude of the steady-state short-circuit current is limited, and the initial phase angle is controlled, which are quite different from those of conventional synchronous generators.

III. Operating Performance Analysis of Distance Protection

Based on the above characteristics of IIREGs, the performance of distance protection configured on the transmission line emanating from the IIREG is analyzed in this section. As illustrated in Fig. 1, Z_W and Z_S are the impedance measured by the distance relays located on the IIREG side and the grid side, respectively.

The occurrence of a short-circuit fault is often accompanied by a fault resistance. Taking an internal fault on the transmission line for instance, the measured impedance detected by the IIREG-side distance relay can be calculated as

$$Z_W = \frac{\dot{U}_m}{\dot{I}_m} = \frac{\dot{I}_m Z_{\mathrm{WK}} + \left(\dot{I}_m + \dot{I}_n\right) R_g}{\dot{I}_m} = Z_{\mathrm{WK}} + Z_{\mathrm{ad}} \quad (3)$$

where $\dot{U}_m$ and $\dot{I}_m$ are the measuring voltage and current detected from the voltage transformer (VT) and the current transformer (CT). For single-phase measuring units, $\dot{U}_m$ and $\dot{I}_m$ are phase voltages and phase currents with zero-sequence compensation, denoted by $\dot{U}_\phi$ and $\dot{I}_\phi + k3\dot{I}_{w0}$, respectively. For polyphase measuring units, they are LL voltages and LL currents. $\dot{I}_{w0}$ is the zero-sequence current on the IIREG side. The zero-sequence compensating factor k can be calculated by $k = (z_0 - z_1)/3z_1$. z_0 and z_1 are the zero- and positive-sequence impedances per unit length of the transmission line. $\dot{I}_n$ is the grid-side current. Z_{WK} is the positive-sequence impedance between the protection and the fault. Z_{ad} is the additional impedance derived from the fault resistance.

As the voltage level of outgoing transmission lines emanating from the IIREG is often above 110 kV, the high-voltage side of the main transformer requires solid grounding; on the contrary, the low-voltage side of the main transformer whose nominal voltage is lower than or equal to 35 kV is in the delta connection mode. Hence, the value of the zero-sequence impedance behind the IIREG-side relay is approximately equal to the main transformer's leakage reactance.

When an ungrounded fault occurs on the outgoing transmission line, due to the lack of the zero-sequence path, the short-circuit current on the IIREG side is completely supplied by the inverter. When any asymmetric ground short-circuit fault occurs, the fault location's zero-sequence voltage and the small zero-sequence impedance lead to a significant zero-sequence current on the IIREG side.

On the above basis, operating performances of conventional distance relays are unveiled in terms of fault types.

A. Three-Phase Short-Circuit Faults

The measured impedance can be obtained by the ground or phase-to-phase impedance relay when a three-phase fault with the fault resistance R_g occurs. The properties of the measured impedance and the performances of the distance relays are analyzed as follows.

1) Ground Impedance Relay: Taking, for instance, a three-phase short-circuit fault, the measured impedance of phase A can be expressed as follows:

$$Z_S = Z_{\mathrm{SK}} + \left(1 + \frac{\dot{I}_{\mathrm{WA}}}{\dot{I}_{\mathrm{SA}}}\right) R_g \quad (4)$$

$$Z_W = Z_{\mathrm{WK}} + \left(1 + \frac{\dot{I}_{\mathrm{SA}}}{\dot{I}_{\mathrm{WA}}}\right) R_g \quad (5)$$

where Z_{SK} is the positive-sequence impedance from the fault location to the relay on the grid side, and $\dot{I}_{\mathrm{WA}}$ and $\dot{I}_{\mathrm{SA}}$ are the faulted phase-A currents of the IIREG side and the grid side, respectively.

Due to the characteristics of the inverter, the short-circuit current is only 1.2–1.5 times the rated current [19], which is much smaller than the short-circuit current of the synchronous generator (approximately ten times the rated current in severe cases). Hence, the ratio $I_{\mathrm{WA}}/I_{\mathrm{SA}}$ is quite small, and the additional impedance is approximately R_g according to (4). Thus, the limited current of the IIREG reduces the impact of the fault resistance on the grid-side measured impedance. As a result, the possibility that the grid-side distance relay refuses to operate for internal faults is greatly reduced.

For (5), due to the large amplitude of $I_{\mathrm{SA}}/I_{\mathrm{WA}}$, the additional impedance value is also large, and its property is governed by the phase of $\dot{I}_{\mathrm{SA}}/\dot{I}_{\mathrm{WA}}$. Because of the time-varying current of IIREGs, the phase of $\dot{I}_{\mathrm{SA}}/\dot{I}_{\mathrm{WA}}$ may vary from 0° to 360° theoretically. If the phase angle is between 0° and 180°, the additional impedance will be expressed as a large inductive one. In consequence, the grid-side distance relay will fail to operate with internal faults. On the other hand, if the phase angle is between 180° and 360°, the additional impedance will be expressed as a large capacitive one, causing the IIREG-side distance relay's misoperation.

For the conventional transmission line connected to double- or multisynchronous generators, quadrilateral distance elements can mitigate the impacts of fault resistance on protection relays. However, for the outgoing transmission line emanating from IIREGs, this improvement will no longer be remarkable. As analyzed above, due to the uncertain phase relationship between the IIREG-side current and the grid-side current, the additional impedance Z_{ad} can be rendered inductive or capacitive rather than purely resistive. The advantage of the quadrilateral distance elements is not prominent under the condition of unclear additional impedance properties. In addition, since the IIREG-side current is limited, the additional impedance value Z_{ad} on this

Authorized licensed use limited to: Washington State University. Downloaded on December 10,2023 at 05:24:04 UTC from IEEE Xplore. Restrictions apply.

side is extremely large. Even if a quadrilateral distance element is used, it still cannot tolerate such a large additional impedance.

Since the quadrilateral distance element has no absolute advantage, the mho element is used in the following analysis. The characteristics of the mho element are clear and intuitive, and its parameters are easy to set. It is representative to study the influence of the fault resistance with mho elements because the resulting properties apply to other distance elements.

2) Phase-to-Phase Impedance Relay: The operating performance analysis method for phase-to-phase impedance relays is similar to the analysis for the ground impedance relays in Section III-A1. The detailed analysis can be found in [19]. It shows that the performance of phase-to-phase impedance relays is similar to that of ground phase relays. The grid-side distance relay will fail to operate with internal faults if the phase angle ranges from 0° to 180°.

B. Phase-to-Phase Short-Circuit Faults

For a short-circuit fault at phases B and C through resistor R_g, the measured impedance can be expressed as follows:

$$Z_S = Z_{\mathrm{SK}} + \frac{\dot{I}_{\mathrm{WB}} + \dot{I}_{\mathrm{SB}}}{\dot{I}_{\mathrm{SB}} - \dot{I}_{\mathrm{SC}}} R_g \tag{6}$$

$$Z_W = Z_{\mathrm{WK}} + \frac{\dot{I}_{\mathrm{WB}} + \dot{I}_{\mathrm{SB}}}{\dot{I}_{\mathrm{WB}} - \dot{I}_{\mathrm{WC}}} R_g. \tag{7}$$

Since the IIREG-side current is far smaller than the grid-side one, (6) can be simplified by $\dot{I}_{\mathrm{WB}} + \dot{I}_{\mathrm{SB}} \approx \dot{I}_{\mathrm{SB}}$, $\dot{I}_{\mathrm{SB}} - \dot{I}_{\mathrm{SC}} \approx 2\dot{I}_{\mathrm{SB}}$, and the additional impedance of the grid side is approximately $0.5R_g$. Thus, the limited current of IIREG reduces the impact of the fault resistance on the measured impedance of the grid side.

Take the control strategy that suppresses the negative-sequence current for instance. Due to the balanced current on the IIREG side, (7) can be simplified by $\dot{I}_{\mathrm{WB}} + \dot{I}_{\mathrm{SB}} \approx \dot{I}_{\mathrm{SB}}$ and $\dot{I}_{\mathrm{WB}} - \dot{I}_{\mathrm{WC}} = \sqrt{3}\dot{I}_{\mathrm{WB}} e^{j30^\circ}$. Therefore, the property of the additional impedance is governed by the phase of $\dot{I}_{\mathrm{SB}}/\dot{I}_{\mathrm{WB}}$. If the phase angle of $\dot{I}_{\mathrm{SB}}/\dot{I}_{\mathrm{WB}}$ ranges from 30° to 210°, the additional impedance will be expressed as a large inductive one. In consequence, the grid-side distance protection will fail to operate for internal faults. In contrast, if the phase angle ranges from −150° to 30°, the additional impedance will be expressed as a large capacitive one. The large capacitive additional impedance would possibly cause the IIREG-side distance relay to misoperate.

C. Two-Phase-to-Ground Short-Circuit Fault

For instance, a phase-B-to-phase-C-to-ground (BCG) fault with fault resistance R_g, the performance of distance protection on both sides is unveiled in this part.

1) Ground Impedance Relay: The phase-B measured impedances of both sides are expressed as follows:

$$Z_S = Z_{\mathrm{SK}} + \frac{\dot{I}_{\mathrm{SB}} + \dot{I}_{\mathrm{WB}}}{\dot{I}_{\mathrm{SB}} + k3\dot{I}_{S0}} R_g \tag{8}$$

$$Z_W = Z_{\mathrm{WK}} + \frac{\dot{I}_{\mathrm{WB}} + \dot{I}_{\mathrm{SB}}}{\dot{I}_{\mathrm{WB}} + k3\dot{I}_{W0}} R_g \tag{9}$$

where $\dot{I}_{S0}$ is the zero-sequence current measured by the grid-side relay.

Due to the limited short-circuit current provided directly by the IIREG with LLG faults, the three-phase currents are full of the zero-sequence component. The IIREG-side equivalent zero-sequence impedance, which is determined by the zero-sequence impedance of the main transformer, is quite larger than the grid equivalent zero-sequence impedance, which is governed by the combination of the external main power lines and transformers. With the amplitude of $\dot{I}_{W0}$ smaller than that of $\dot{I}_{S0}$, the grid-side additional impedance value is generally less than R_g, while the IIREG-side additional impedance value is greater than R_g. When there is a fault in the protective zone, distance relay on the grid side can often reliably operate, whereas distance relay on the IIREG side may refuse to operate.

2) Phase-to-Phase Impedance Relay: The analysis here is basically the same as the analysis of the phase-to-phase impedance relay for the three-phase short circuit. Like other faults, the possibility that the grid-side distance relay fails to operate for internal faults is greatly reduced and the IIREG-side distance relay can operate with the possibility of overreaching.

To sum up, with various types of short-circuit faults, because of the limited amplitude of the short-circuit current and the controlled initial phase angle, the additional impedance on the grid side is almost purely resistive, and its value is no bigger than the fault resistance, making the distance relay operate more reliably. In contrast, the additional impedance on the IIREG side can be inductive or capacitive, and its value can be rather bigger than the fault resistance, causing the distance relay to misoperate.

IV. Improvement of the Protection Scheme

According to the above analysis in Section III, a delay element can be applied to make the IIREG-side distance relay out of operation for a short period of time. During this short period of time, the grid-side relay that can correctly reflect faults is still in service. After the relay on the grid side operates reliably, the transmission line and the IIREG form a single-ended network. At this time, with no grid-side boosting current, the IIREG-side distance relay can correctly reflect the fault.

For ungrounded short-circuit faults on the line, the short-circuit current provided by the IIREG side is very small, which is no more than 1.5 times rated current according to analysis in Section II, and therefore, short-term blocking will not cause serious consequences. However, for asymmetric ground short circuit on the line, the IIREG side will also provide significant zero-sequence current; the utilization of postponement program to avoid malfunction is not desirable. At this point, zero-sequence electric quantities could be utilized to improve the performance of the IIREG-side protection. Since the operation condition of the equivalent grid is unknown, it will be difficult to set the threshold of the zero-sequence current as a discriminant quantity. Hence, it is suggested to add a zero-sequence distance protection as a supplement on the renewable energy generator side.

Since only the fault point is a zero-sequence excitation source, the impedance reflected by the zero-sequence distance relay

Authorized licensed use limited to: Washington State University. Downloaded on December 10,2023 at 05:24:04 UTC from IEEE Xplore. Restrictions apply.

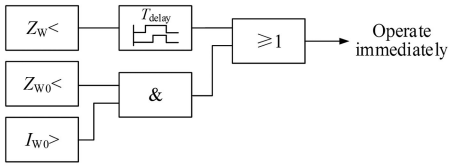

Fig. 2. Improved scheme for the IIREG-side protection.

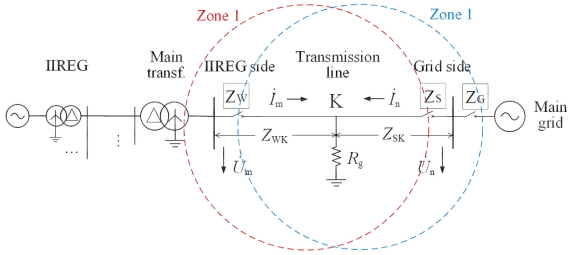

Fig. 3. Zonal configuration of relays on both sides of transmission line.

Z_{W0} is the opposite value of the main transformer zero-sequence impedance $Z_{\text{transf.0}}$, that is, $Z_{W0} = -Z_{transf.0}$. Therefore, a zero-sequence distance relay is used as a judgment element for a ground short-circuit fault. It should be noted that, even if an ungrounded fault occurs, a transient zero-sequence current can also be detected immediately after the fault inception. In addition, under normal operating conditions, the measured zero-sequence voltage and current are both almost zero. The calculated zero-sequence impedance value is irregular and meaningless, which may lead to malfunction of the zero-sequence distance relay. Hence, apart from configuring the zero-sequence distance relay, it is necessary to add a zero-sequence overcurrent relay as a starting element to avoid malfunction.

As shown in Fig. 2, the conventional distance relay and the zero-sequence distance relay accompanied by a zero-sequence overcurrent starting element constitute the main protection on the IIREG side.

The following is a detailed analysis on the performance of the improved protection scheme when a variety of short-circuit faults occur on the outgoing transmission line.

A. Ungrounded Short-Circuit Faults

Consider the situation that a phase-B-to-phase-C short-circuit fault with the fault resistance occurs on the outgoing transmission line.

To protect the entire transmission line, the action impedance of the zone 1 distance relay on the grid side $Z_{\text{act}.g}$ is set using the positive-sequence impedance of the line, denoted by Z_L. Here, the conventional zone 1 distance protection's limit that can only protect 85% to 95% of the line in length is overcome due to the main transformer behind the IIREG-side bus. The main transformer's impedance Z_{transf} is approximately several tens of ohm, which is much larger than the impedance of the transmission line per unit length. As a result, when short-circuit faults occur behind the main transformer, the measured impedance on the grid side is at least $Z_L + Z_{\text{transf}}$. The value is much larger than the action impedance $Z_{\text{act}.g}$. Therefore, as shown in Fig. 3, given the measurement errors of the VTs and CTs, 1.3 times the line positive-sequence impedance is taken for zone 1 protection, and zone 2 distance protection is not required due to the fact that the first zone can cover the whole protected line. According to the analysis in Section III, the grid-side relay can identify the fault near this border precisely and quickly. Hence, the grid-side zone 1 distance protection can operate instantaneously for any internal faults.

After the grid-side distance relay operates and the main grid system is isolated, the IIREG, the transmission line, and the fault location form a single-ended power failure network. At this moment, no matter what kind of control strategy is taken by the inverter, as long as short-circuit current injected into the fault location from the IIREG side, the measured power-frequency-based impedance can be derived by (10), and the distance relay configured on this side can operate correctly

$$Z_W = \frac{\dot{U}_m}{\dot{I}_m} = Z_{\text{WK}} + R_g. \tag{10}$$

Therefore, the action impedance of the IIREG-side distance relay can be set based on this. This relay should not be put into use until the main grid system is isolated. It can coordinate with the lower order distance relay Z_G with time coordination. Therefore, the protective range of the IIREG-side distance relay can also reach the entire transmission line. Taking into account the errors and the safety margin, 1.3 times the line positive-sequence impedance is applied in this paper.

B. Ground Short-Circuit Faults

When any point of the outgoing transmission line is ground short-circuited with the fault resistance, due to the relatively small zero-sequence impedance, which only includes the impedance of the main transformer and the transmission line from the relay to the fault location, the fault current is mainly zero-sequence component one. Hence, the significant zero-sequence current is able to activate the zero-sequence distance relay on the IIREG side. The zero-sequence impedance Z_{W0} can be expressed by (11). The trace of Z_{W0} enters the impedance circle range, which is set as $-1.3Z_{\text{transf.0}}$ in this paper, and then, the IIREG-side protection sends the tripping signal. At the same time, as little affected by the fault resistance, the impedance trace on the grid side enters the operating zone, and the grid-side relay sends the tripping signal instantaneously

$$Z_{W0} = \frac{\dot{U}_{m0}}{\dot{I}_{m0}} = -Z_{\text{transf. 0}} \approx -jX_s. \tag{11}$$

In (11), the subscript 0 represents zero-sequence electrical quantities; $Z_{\text{transf.0}}$ and X_s are the zero-sequence impedance and the leakage reactance of the main transformer, respectively.

V. Simulation Verification and the Field Test

A. Simulation Verification

To validate the operating performance of the distance protection, simulation verification has been carried out. The hardware platform used in the simulation is composed of a main controller, a monitor, a pulsewidth modulation generator, and a real-time digital simulator (RTDS) developed by RTDS Technologies,

Authorized licensed use limited to: Washington State University. Downloaded on December 10,2023 at 05:24:04 UTC from IEEE Xplore. Restrictions apply.

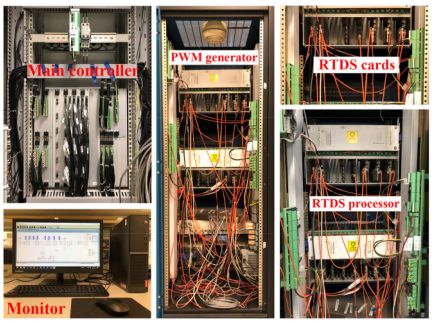

Fig. 4. Physical layout of the experimental test system.

TABLE I
PARAMETERS OF A SINGLE IIREG

Element	Parameter	Value
Inverter	Rated power	1.5 MW
	Rated voltage	2.2 kV
	Proportional gain of voltage/current controller	0.75 / 0.329 p.u.
	Integration time constant of voltage/current controller	0.875 / 0.018 p.u.
DC-link	Rated voltage	1.2 kV
	Capacitor	4500 μF
Filter	Capacitor	200 μF
	Inductance on IIREG/grid side	1100 / 124 μH

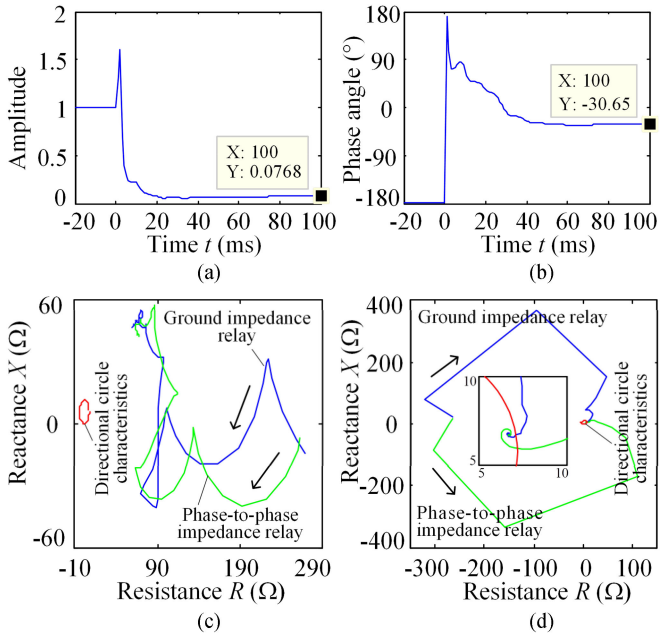

Fig. 5. Impedance calculated by the AG element and the BC element when a three-phase fault with a 5-Ω resistance occurs on the middle of the outgoing transmission line. (a) Amplitude of phasor $\dot{I}_{\mathrm{WA}}/\dot{I}_{\mathrm{SA}}$. (b) Phase of phasor $\dot{I}_{\mathrm{WA}}/\dot{I}_{\mathrm{SA}}$. (c) Measured impedance on the IIREG side. (d) Measured impedance on the grid side.

which is depicted in Fig. 4. The role of these components can be found in [30]. The model built on the RTDS is shown in Fig. 1. Its parameters are evaluated from the actual values of the IIREG. The rating values for a single IIREG are 1.5 MW and 0.69 kV. The voltage of the inverter is oriented to the d^+-axis. The target active and reactive power commands are $P_0^* = e_d^+$ and $Q_0^* = 1.5e_d^+(0.9 - e_d^+)$. The maximum allowable value of the inverter current is $1.5I_N$. The other parameters of the IIREG are detailed in Table I. The 1.6-MVA 35/0.69-kV step-up transformer with capacity expansion is in wye-delta (ground in the wye side) connection, and its reactance is 6.76%. The expansion ratio in the simulation is 1:132, that is, the total capacity of the IIREGs is $1.5 \times 132 = 198$ MW. The equivalent resistance and inductance of the collection line is 0.275 Ω and 1024 μH, respectively. The 200-MVA 220/35-kV main transformer is in wye-delta (ground in the wye side) connection, and its reactance is 6%. The positive- and zero-sequence impedance and capacitance of the 40-km transmission line are $0.076 + j0.338$ Ω/km and $0.284 + j0.824$ Ω/km and 0.0086 μF/km and 0.0061 μF/km, respectively. The equivalent positive- and zero-sequence impedance of the grid are both $0.2 + j6.283$ Ω.

Mho impedance elements whose acting impedance is $1.3Z_L$ are applied. Hence, the protective range of zone 1 distance relay can reach 100% of the length of the transmission line. The block time of the IIREG-side distance protection should include the grid-side relay-operating time $t_{\mathrm{rel}.g}$, the time $t_{\mathrm{bk}.g}$ for circuit breaker to enable isolation of the trouble area, and the dynamic adjustment time $t_{\mathrm{ad}.f}$ of the inverter output current. The typical values for these times are $t_{\mathrm{rel}.g} = 50$ ms, $t_{\mathrm{bk}.g} = 80$ ms [8], and $t_{\mathrm{ad}.f} = 20$ ms. To ensure that the grid-side boosting current is interrupted completely, the delay of distance relay on the IIREG side in the simulation is taken as $t_{\mathrm{delay}.f} = 0.3$ s. In the following simulations in Sections V-A1–V-A3, the faults occur at the midpoint of the transmission line. The impacts of different fault locations on the protection performance are analyzed in Sections V-A4.

1) Three-Phase Short-Circuit Faults: Taking, for instance, a three-phase short-circuit fault with the 5-Ω resistance, the amplitude and phase of phasor $\dot{I}_{\mathrm{WA}}/\dot{I}_{\mathrm{SA}}$ and measured impedance on both sides are depicted in Fig. 5.

It is known from Fig. 5(a) and (b) that consistent with the aforementioned theoretical analysis, the amplitude of $\dot{I}_{\mathrm{WA}}/\dot{I}_{\mathrm{SA}}$ is 0.07683, which is far smaller than 1, and the phase of $\dot{I}_{\mathrm{WA}}/\dot{I}_{\mathrm{SA}}$ is $-30.65°$. Thus, the measured impedance on the IIREG side is large enough that its trace does not enter the operating zone, which is shown in Fig. 5(c). Accordingly, the distance relay on this side may refuse to operate for internal faults. In contrast, the measured impedance's trace of the grid side finally enters the operating zone, as shown in Fig. 5(d). As a result, the zone 1 distance protection on this side can operate reliably.

Analyze Fig. 5(c) and (d) for further information. In the transient process, the measured impedance of ground or phase-to-phase relay changes irregularly due to the pre- and postfault sampling values. However, after entering the steady state, they are basically close to each other. It verifies the viewpoint that the connecting method of distance relay has a little impact on the protection's performance with three-phase short-circuit faults.

Apply the improved program described in Section IV. After the fault occurs, the distance relay on the grid side operates immediately. After the grid-side protection isolates the grid-side system, the inverter supplies limited short-circuit current

Authorized licensed use limited to: Washington State University. Downloaded on December 10,2023 at 05:24:04 UTC from IEEE Xplore. Restrictions apply.

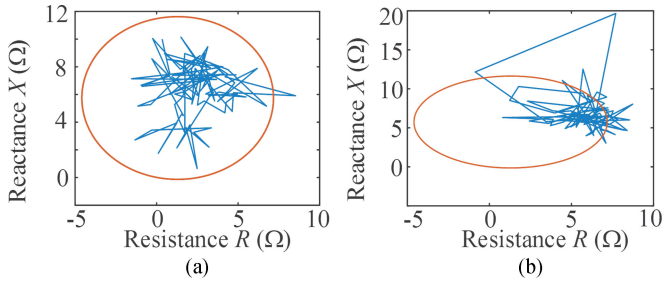

Fig. 6. Trace of the IIREG-side impedance (0.3 s after phase-to-phase short-circuit faults). (a) With a three-phase fault with a 5-Ω resistance on the middle of the outgoing line. (b) With a BC fault with a 5-Ω resistance on the middle of the outgoing line.

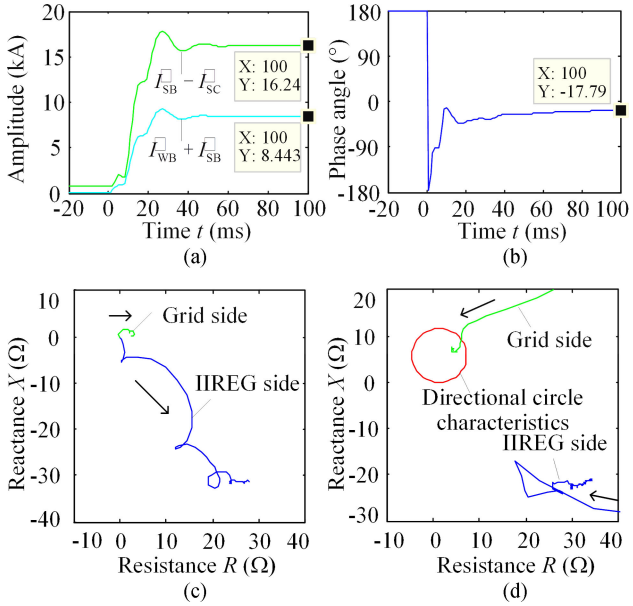

Fig. 7. Fault features and operating performance of distance relay when a BC fault with a 5-Ω resistance occurs on middle of the outgoing transmission line. (a) Amplitude of the current phasor. (b) Phase of the phasor $\dot{I}_{\mathrm{SB}}/\dot{I}_{\mathrm{WB}}$. (c) Trace of the additional impedance. (d) Trace of the measured impedance.

to the transmission line. After a delay time of 0.3 s, the IIREG-side distance relay is put into service. Due to the lack of voltage support from the ac system, the short-circuit current provided by the inverter has serious distortion. Therefore, the trace of the measured impedance is not stable at that time. However, as shown in Fig. 6(a), the trace basically falls inside the impedance circle; then, the protection can operate correctly.

2) Phase-to-Phase Short-Circuit Faults: The characteristics of the phase-B-to-phase-C fault with the 5-Ω resistance and the operating performance of distance relay are illustrated in Fig. 7.

As observed from Fig. 7(a), consistent with the theoretical analysis, the amplitude of $\dot{I}_{\mathrm{WB}}+\dot{I}_{\mathrm{SB}}$ is approximately half of the value of $\dot{I}_{\mathrm{SB}}-\dot{I}_{\mathrm{SC}}$, making the additional impedance of the grid side almost purely resistive. According to Fig. 7(c), the steady-state value of the additional impedance is $2.59+j0.15\,\Omega$, which is very close to the theoretical value of $0.5R_g=2.5\,\Omega$.

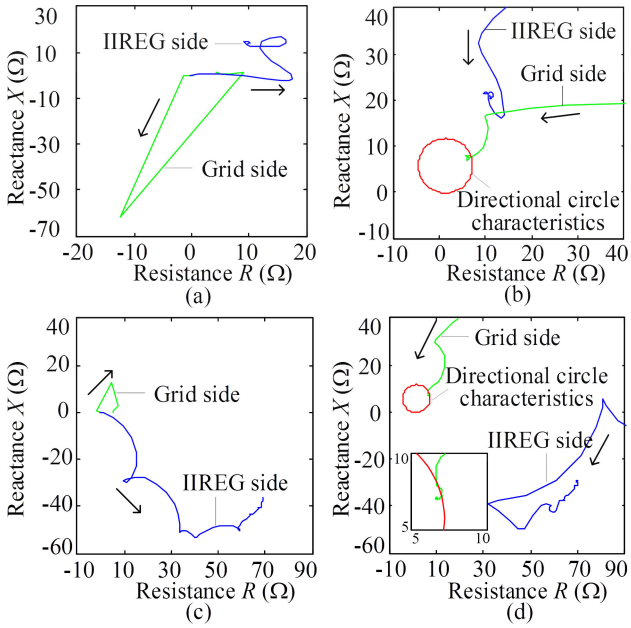

Fig. 8. Operating performance of distance relay when a BCG fault with a 5-Ω resistance occurs on the middle of outgoing transmission line. (a) Additional impedance calculated by the AG element. (b) Measured impedance measured by the AG element. (c) Additional impedance calculated by the BC element. (d) Measured impedance measured by the BC element.

Under this circumstance, the measured impedance's trace can enter the operating zone, which is shown in Fig. 7(d), and the zone 1 distance protection can operate reliably.

For the IIREG side, as shown in Fig. 7(b), the angle of the phasor $\dot{I}_{\mathrm{SB}}/\dot{I}_{\mathrm{WB}}$ is $-17.79°$. Thus, the additional impedance on this side appears to be resistive and capacitive, and its steady-state value, illustrated in Fig. 7(c), is $27.89-j31.19\ \Omega$. Its trace cannot fall into the operating zone. Therefore, the zone 1 distance protection refuses to operate for internal faults.

After IIREG-side protection is out of service for a short term and zero-sequence distance relay accompanied by a zero-sequence over-current starting element is configured, because the zero-sequence distance relay cannot be activated due to no steady zero-sequence current, only the grid-side distance relay can operate immediately under a two-phase short-circuit fault. After a delay of 0.3 s, the IIREG-side distance relay is re-enabled. Like three-phase short-circuit faults, the IIREG-side short-circuit current with distortion leads to the constant change of the measured impedance's trace. However, as shown in Fig. 6(b), most of the trace still fall into the impedance circle, so the relay can operate accurately.

3) Phase-to-Phase-to-Ground Short-Circuit Faults: Fig. 8 shows the additional impedance and measured impedance with the two types of wiring mode when a BCG fault with 5-Ω resistance occurs.

It is known from Fig. 8(a) that for the ground impedance relay, consistent with the theoretical analysis, the steady-state values of the additional impedance on the grid side and the IIREG side are $4.61+j0.94\ \Omega$ and $9.64+j13.44\ \Omega$, respectively. As shown in Fig. 8(b), the measured impedance's trace of the

Authorized licensed use limited to: Washington State University. Downloaded on December 10,2023 at 05:24:04 UTC from IEEE Xplore. Restrictions apply.

TABLE II
MEASURED IMPEDANCE OF DISTANCE RELAYS ON BOTH SIDES WITH DIFFERENT FAULT LOCATIONS

Fault locat.	Fault resist. (Ω)	Fault type	The grid-side distance relay		The IIREG-side distance relay [a]	
			R+jX (Ω)	Result [b]	R+jX (Ω)	Result [c]
K0	0	BC	23.67+j26.48	×	--	×
		ABC	3.44+j28.63	×	--	×
K1	5	BC	8.01+j13.10	√	5.06+j0.44	√
		ABC	8.00+j13.09	√	5.10+j0.44	√
K2	5	BC	7.48+j10.81	√	5.42+j2.30	√
		ABC	7.49+j10.79	√	5.44+j2.84	√
K3	5	BC	6.58+j6.78	√	5.96+j6.32	√
		ABC	6.57+j6.77	√	5.73+j7.10	√
K4	5	BC	5.62+j2.74	√	7.43+j10.82	√
		ABC	5.63+j2.71	√	5.64+j12.15	√
K5	5	BC	5.10+j0.57	√	7.54+j12.47	√
		ABC	5.08+j0.51	√	7.12+j13.43	√

[a] The data of the IIREG side are the measured values at 0.3 s after the faults.
[b,c] Judgments whether the fault is in the operating zone.

TABLE III
MEASURED IMPEDANCE OF DISTANCE RELAYS ON BOTH SIDES WITH DIFFERENT FAULT RESISTANCES

Fault resist. (Ω)	The grid-side distance relay		The IIREG-side distance relay [d]	
	R+jX (Ω)	Result [e]	R+jX (Ω)	Result [f]
0.1	2.58+j10.76	√	0.45+j2.47	√
1	3.48+j10.78	√	1.52+j2.41	√
2	4.48+j10.77	√	2.57+j2.88	√
5	7.48+j10.81	√	5.42+j2.30	√
8	10.47+j10.84	√	8.58+j2.73	√
10	12.49+j10.81	×	--	×

[d] The data of the IIREG side are the measured values at 0.3 s after the faults.
[e,f] Judgments whether the fault is in the operating zone.

grid side can enter the inside of the operating zone, causing the zone 1 distance protection's reliable operation. In contrast, the measured impedance's trace of the IIREG side fails to enter the operating zone, so the operation refuses to operate. Fig. 8(c) and (d) shows the additional impedance and measured impedance calculated by the BC element. The conclusions are similar to that reflected by the AG impedance element.

If the zero-sequence distance relay with zero-sequence overcurrent starting element is equipped, the zero-sequence current of ground faults is big enough to start zero-sequence distance relay. Before the circuit breaker successfully interrupts the short-circuit current on the grid side, the IIREG-side zero-sequence impedance is approximately $-j14.5\ \Omega$, which can enter the operating zone stably and trigger the protection's correct operation.

Based on the above simulation results, the tripping time for each relay under a typical short-circuit condition can be obtained. The results reflect that within 0.3 s after faults, relays configured on both sides of the outgoing line can send the correct trip command.

4) Influence of Different Fault Locations: In order to study the impact of the fault location on the protective scheme, faults were set at 3%, 20%, 50%, 80%, and 97% the length of the transmission line from the main transformer of the IIREG. These five fault locations were marked in order as K1–K5. A fault located at the line connected to the low-voltage side (35 kV) of the main transformer was represented by K0, and this fault is 0.1% line length from the transformer. For the grid-side distance relay, K1–K5 were internal faults and K0 was an external fault. Fault types at each location include the three-phase short circuit and the phase-B-to-phase-C short circuit with the 5-Ω resistance. The measured impedances of the phase-to-phase impedance relay are shown in Table II.

According to Table II, for both types of phase faults located from K1 to K5, all the phase-to-phase relays can operate reliably, and these faults are identified as internal ones. For external faults that are marked as K0, distance relays can reliably avoid malfunction. If the faults close to both ends of the protected line and the faults in the middle of the line can be distinguished, then other fault locations with all types of faults can be inferred based on the results derived from these typical six locations.

5) Influence of Different Fault Resistances: In addition to verifying the impact of fault locations on the protection scheme, the effect of fault resistance at a typical location (K2, 20% of the line length from the IIREG bus) is investigated. Given that the largest fault resistance for the 220-kV transmission-line phase-to-phase fault is a dozen or so ohm, the fault resistances in the simulation were set to 0.1, 1, 2, 5, 8, and 10 Ω, respectively. The measured impedance of the phase-to-phase impedance relay is shown in Table III.

From Table III, it is obvious that unless the fault resistance is particularly large, the measured impedance's trace of the proposed scheme is in the mho characteristic circle, and therefore, the relay can correctly identify the internal faults. If the robustness of the relatively rare large fault resistance has to be considered, a quadrilateral type distance characteristic relay can be used.

B. Field Test

To further verify the feasibility of the above-mentioned improvement scheme, a short-circuit test was conducted on the outgoing line of a renewable energy power station in Jilin Province, China. The renewable energy power station is a type-IV WF equipped with permanent-magnet direct-drive synchronous generators, whose fault characteristics correspond to those discussed in Section II. The WF is currently equipped with 90 wind driven generators with a total installed capacity of 135 MW (90 × 1.5 MW). The primary connection mode is the same as that depicted in Fig. 1. The power generated by the wind-driven generators is sent by the main transformer after it passes through the collection system. The rated capacity of the main transformer is 200 MVA, and the rated voltage is 220/35 kV. In order to prevent the switching of the WFs from affecting the zero-sequence impedance, the 220-kV side of the main transformer is grounded via a discharging gap. The outgoing line's rated voltage is 220 kV, and its total length is 54.927 km. The fault in the test is set as a phase-A-to-ground short circuit occurred approximately 22 km from the WF.

Curves of the IIREG-side instantaneous current $i_{\varphi}(t)$ and zero-sequence current I_0, which are based on the live recording

Authorized licensed use limited to: Washington State University. Downloaded on December 10,2023 at 05:24:04 UTC from IEEE Xplore. Restrictions apply.

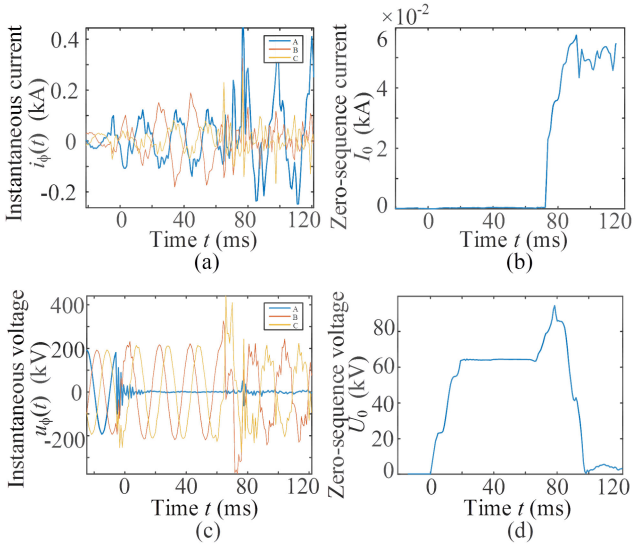

Fig. 9. IIREG-side voltage and current waveforms based on the live recording data. (a) Instantaneous current value. (b) Zero-sequence current (rms). (c) Instantaneous voltage value. (d) Zero-sequence voltage (rms).

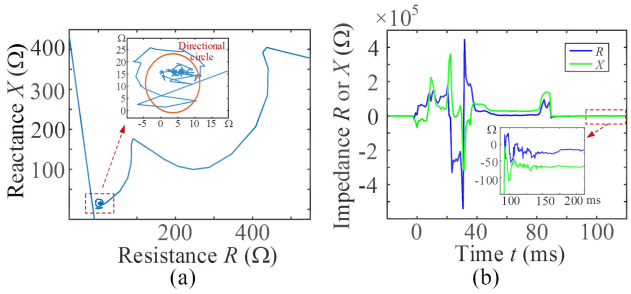

Fig. 10. (a) Trace of the grid-side impedance. (b) Waveform of the IIREG-side impedance.

data, are shown in Fig. 9(a) and (b). The zero-sequence current I_0 appears at approximately 70 ms after the fault because the discharging gap on the 220-kV side of the main transformer cannot be immediately punctured after the fault.

Fig. 9(c) and (d) shows the waveforms of the IIREG-side instantaneous voltage $u_\varphi(t)$ and zero-sequence voltage U_0. After the short-circuit fault, the voltage of phase A is attenuated to a minuscule value, and voltages of phases B and C remain almost unchanged (in fact, they increase slightly). These phenomena are similar to the fault condition for direct grounded system, in which a single phase is shorted to ground. However, as mentioned in the previous paragraph, within 70 ms after the occurrence of the short circuit, the main transformer's discharging gap has not been broken down, so the grounding mode is equivalent to the neutral point being ungrounded. The reason for the appearance of the voltage waveform shown in the Fig. 9(c) needs further analysis.

Before the discharging gap is punctured, the zero-sequence impedance on the IIREG side is infinite. The equivalent impedance outside the fault point is the parallel value of the grid-side impedance and the IIREG-side impedance. Therefore, the equivalent zero-sequence impedance outside the fault point is approximately the grid-side zero-sequence impedance. For a single-phase-to-ground short circuit, all the three-sequence currents at the fault point are equal, and the fault-phase voltage is zero. In the general case where the zero-sequence impedance is slightly greater than the positive- and negative-sequence one, the unfaulted-phase voltage rises slightly. Because the limited short-circuit current on the IIREG side produces a little voltage drop on the transmission line, the measured voltage on this side is similar to that at the fault point, according to the waveform shown in Fig. 9(c). When the discharging gap is broken down, the zero-sequence current surges, and the zero-sequence voltage on the IIREG side is no longer that at the fault point but decreases to the voltage on the main transformer's leakage impedance, as shown in Fig. 9(d).

Fig. 10(a) shows the impedance diagram on the grid side. According to the R–X diagram, the distance protection can operate quickly and accurately. Based on the above improved scheme, the zero-sequence distance relay with a zero-sequence overcurrent starting element is adopted on the IIREG side for single-phase-to-ground faults. The zero-sequence impedance's waveforms before and after the fault are shown in Fig. 10(b). After the discharging gap is broken down, the zero-sequence impedance is approximately equal to the main transformer's leakage impedance (a part of the resistance also corresponds to the arc at the discharging gap). Thus, the distance protection based on the zero-sequence impedance can correctly reflect the fault and operate. The time taken for the protection's action is about 150 ms, which satisfies the quickness requirement of protection.

VI. Conclusions

In this paper, by analyzing the characteristics of the short-circuit current provided by IIREG, the viewpoint is theoretically deduced that due to the influence of the grid-side boosting current, the measured impedance of the IIREG side has a great amplitude and phase offset, which causes the conventional distance protection to malfunction or refuse to operate. To solve this problem, an improved scheme based on delay and zero-sequence impedance was proposed. The scheme can accurately identify the fault location without obtaining the electrical quantities on the opposite side by communication.

By assuming various types of faults such as ground and ungrounded short circuit, simulation results confirm the defects of the existing distance protection and validate the wide applicability of the proposed improved scheme. The simulation results show that the proposed scheme can clearly distinguish between internal and external faults and has great adaptability to fault resistance.

After verification by simulation, the field test was conducted. The test results show that the improved distance protection can quickly identify internal faults and meet the requirements of speed and selectivity, which reflects the engineering application value of the improved scheme.

Authorized licensed use limited to: Washington State University. Downloaded on December 10,2023 at 05:24:04 UTC from IEEE Xplore. Restrictions apply.

REFERENCES

[1] A. S. Brouwer *et al.*, "Operational flexibility and economics of power plants in future low-carbon power systems," *Appl. Energy*, vol. 156, pp. 107–128, 2015, doi: 10.1016/j.apenergy.2015.06.065.

[2] T. Broeer *et al.*, "A demand response system for wind power integration: Greenhouse gas mitigation and reduction of generator cycling," *CSEE J. Power Energy Syst.*, vol. 4, no. 2, pp. 121–129, Jun. 2018, doi: 10.17775/CSEEJPES.2018.00500.

[3] O. Noureldeen and I. Hamdan, "Design of robust intelligent protection technique for large-scale grid-connected wind farm," *Protection Control Modern Power Syst.*, vol. 3, no. 1, p. 17, Jun. 2018, doi: 10.1186/s41601-018-0090-4.

[4] Z. Chen *et al.*, "Intelligent fault diagnosis of photovoltaic arrays based on optimized kernel extreme learning machine and I-V characteristics," *Appl. Energy*, vol. 204, pp. 912–931, 2017, doi: 10.1016/j.apenergy.2017.05.034.

[5] P. S. Georgilakis, "Technical challenges associated with the integration of wind power into power systems," *Renew. Sustain. Energy Rev.*, vol. 12, no. 3, pp. 852–863, 2008, doi: 10.1016/j.rser.2006.10.007.

[6] A. S. El-Din *et al.*, "Comparing socioeconomic & environmental impacts of building 2GW PV power plant in both sides of the Medeterranian," in *Proc. 1st Int. Renew. Sustain. Energy Conf.*, 2013, pp. 331–336, doi: 10.1109/IRSEC.2013.6529736.

[7] U.S. NREL, "20% wind energy by 2030: Increasing wind energy's contribution to U.S. electricity supply," U.S. DOE Report, Jul. 2008. [Online]. Available: https://www.nrel.gov/docs/fy08osti/41869.pdf

[8] J. L. Blackburn and T. J. Domin, *Protective Relaying: Principles and Applications*, 3rd ed. Boca Raton, FL, USA: CRC Press, 2006.

[9] H. Song and K. Nam, "Dual current control scheme for PWM converter under unbalanced input voltage conditions," *IEEE Trans. Ind. Electron.*, vol. 46, no. 5, pp. 953–959, Oct. 1999, doi: 10.1109/41.793344.

[10] N. Nimpitiwan, G. T. Heydt, R. Ayyanar, and S. Suryanarayanan, "Fault current contribution from synchronous machine and inverter based distributed generators," *IEEE Trans. Power Del.*, vol. 22, no. 1, pp. 634–641, Jan. 2007, doi: 10.1109/TPWRD.2006.881440.

[11] N. Arghira *et al.*, "Aspects regarding integration of wind power plants into the power system," in *Proc. 9th WSEAS Int. Conf. Power Syst.*, 2009, pp. 127–131.

[12] W. Wei, L. Zhang, B. Gao, Y. Tang, N. Chen, and L. Zhu, "Frequency inconsistency in DFIG-based wind farm during outgoing transmission line faults and its effect on longitudinal differential protection," in *Proc. 4th Annu. IEEE Int. Conf. Cyber Technol. Automat., Control Intell.*, 2014, pp. 25–30, doi: 10.1109/CYBER.2014.6917430.

[13] M. Singh, "Protection coordination in distribution systems with and without distributed energy resources—A review," *Protection Control Modern Power Syst.*, vol. 2, no. 1, pp. 1–27, 2017, doi: 10.1186/s41601-017-0061-1.

[14] S. Shen and P. Zhang, "Characteristics of sequence impedances of DFIG wind farm and the impacts on the phase selection elements," in *Proc. IEEE PES Gen. Meeting Conf. Expo.*, 2014, pp. 1–5, doi: 10.1109/PESGM.2014.6938876.

[15] A. Hooshyar, M. A. Azzouz, and E. F. El-Saadany, "Distance protection of lines connected to induction generator-based wind farms during balanced faults," *IEEE Trans. Sustain. Energy*, vol. 5, no. 4, pp. 1193–1203, Oct. 2014, doi: 10.1109/TSTE.2014.2336773.

[16] H. Sadeghi, "A novel method for adaptive distance protection of transmission line connected to wind farms," *Int. J. Elect. Power Energy Syst.*, vol. 43, no. 1, pp. 1376–1382, Dec. 2012, doi: 10.1016/j.ijepes.2012.06.072.

[17] S. I. Jang, J. H. Choi, J. W. Kim, and D. M. Choi, "An adaptive relaying for the protection of a wind farm interconnected with distribution networks," in *Proc. IEEE PES Transmiss. Distrib. Conf. Expo.*, 2003, vol. 1, pp. 296–302, doi: 10.1109/TDC.2003.1335238.

[18] S. Chen, N. Tai, C. Fan, J. Liu, and S. Hong, "Adaptive distance protection for grounded fault of lines connected with doubly-fed induction generators," *IET Gener., Transmiss. Distrib.*, vol. 11, no. 6, pp. 1513–1520, Apr. 2017, doi: 10.1049/iet-gtd.2016.1145.

[19] A. Hooshyar, M. A. Azzouz, and E. F. El-Saadany, "Distance protection of lines emanating from full-scale converter-interfaced renewable energy power plants—Part I: Problem statement," *IEEE Trans. Power Del.*, vol. 30, no. 4, pp. 1770–1780, Aug. 2015, doi: 10.1109/TPWRD.2014.2369479.

[20] Y. Q. Xia, K. K. Li, and A. K. David, "Adaptive relay setting for stand-alone digital distance protection," *IEEE Trans. Power Del.*, vol. 9, no. 1, pp. 480–491, Jan. 1994, doi: 10.1109/61.277720.

[21] A. K. Pradhan and G. Joos, "Adaptive distance relay setting for lines connecting wind farms," *IEEE Trans. Energy Convers.*, vol. 22, no. 1, pp. 206–213, Mar. 2007, doi: 10.1109/TEC.2006.889621.

[22] A. Hooshyar, M. A. Azzouz, and E. F. El-Saadany, "Distance protection of lines emanating from full-scale converter-interfaced renewable energy power plants—Part II: Solution description and evaluation," *IEEE Trans. Power Del.*, vol. 30, no. 4, pp. 1781–1791, Aug. 2015, doi: 10.1109/TPWRD.2014.2369480.

[23] K. Jia *et al.*, "Transient current similarity based protection for wind farm transmission lines," *Appl. Energy*, vol. 225, pp. 42–51, Sep. 2018, doi: 10.1016/j.apenergy.2018.05.012.

[24] M. K. Jena and S. R. Samantaray, "Data-mining-based intelligent differential relaying for transmission lines including UPFC and wind farms," *IEEE Trans. Neural Netw. Learn. Syst.*, vol. 27, no. 1, pp. 8–17, Jan. 2016, doi: 10.1109/TNNLS.2015.2404775.

[25] V. Telukunta, J. Pradhan, A. Agrawal, M. Singh, and S. G. Srivani, "Protection challenges under bulk penetration of renewable energy resources in power systems: A review," *CSEE J. Power Energy Syst.*, vol. 3, no. 4, pp. 365–379, Dec. 2017, doi: 10.17775/CSEEJPES.2017.00030.

[26] R. Kabiri, D. G. Holmes, and B. P. McGrath, "Control of active and reactive power ripple to mitigate unbalanced grid voltages," *IEEE Trans. Ind. Appl.*, vol. 52, no. 2, pp. 1660–1668, Mar./Apr. 2016, doi: 10.1109/TIA.2015.2508425.

[27] J. Jia, G. Yang, A. H. Nielsen, and P. R. Hansen, "Impact of VSC control strategies and incorporation of synchronous condensers on distance protection under unbalanced faults," *IEEE Trans. Ind. Electron.*, vol. 66, no. 2, pp. 1108–1118, Feb. 2019, doi: 10.1109/TIE.2018.2835389.

[28] K. Jia, C. Gu, Z. Xuan, L. Li, and Y. Lin, "Fault characteristics analysis and line protection design within a large-scale photovoltaic power plant," *IEEE Trans. Smart Grid*, vol. 9, no. 5, pp. 4099–4108, Sep. 2018, doi: 10.1109/TSG.2017.2648879.

[29] J. Jia, G. Yang, and A. H. Nielsen, "A review on grid-connected converter control for short-circuit power provision under grid unbalanced faults," *IEEE Trans. Power Del.*, vol. 33, no. 2, pp. 649–661, Apr. 2018, doi: 10.1109/TPWRD.2017.2682164.

[30] S. Liu *et al.*, "Coordinated fault-ride-through strategy for doubly-fed induction generators with enhanced reactive and active power support," *IET Renew. Power Gener.*, vol. 10, no. 2, pp. 203–211, Feb. 2016, doi: 10.1049/iet-rpg.2015.0003.

Yu Fang received the B.Eng. degree in electrical engineering in 2017 from North China Electric Power University, Beijing, China, where he is currently working toward the M.Eng. degree in electrical engineering.

His current research interests include analysis of power systems with renewable energy and power system protection and control.

Ke Jia (M'18) was born in China in 1986. He received the M.Sc. and Ph.D. degrees in electrical engineering from Nottingham University, Nottingham, U.K., in 2008 and 2011, respectively.

He then worked as a Research Fellow with Nottingham University until 2013. He is currently an Associate Professor with North China Electric Power University, Beijing, China. His research interests include power system protection and fault location, microgrid automation, and renewable energy.

Authorized licensed use limited to: Washington State University. Downloaded on December 10,2023 at 05:24:04 UTC from IEEE Xplore. Restrictions apply.

Zhe Yang was born in China in 1994. He received the bachelor's degree in electrical engineering in 2017 from Northeast Electric Power University, Beijing, China, where he is currently working toward the master's degree in electrical engineering.

His research interests include power system protection and control, fault location, and renewable energy.

Yanbin Li was born in China in 1989. He received the Ph.D. degree in electrical engineering from North China Electric Power University, Beijing, China, in 2018.

He is currently with the North China Branch of State Grid Corporation of China, Beijing. His research interests include power system protection and control.

Tianshu Bi (M'98–SM'09) received the Ph.D. degree in electrical and electronic engineering from the University of Hong Kong, Hong Kong, in 2002.

She is currently a Professor with North China Electric Power University, Beijing, China. Her research interests include power system protection and control and synchronized phasor measurement technique and its application.

Authorized licensed use limited to: Washington State University. Downloaded on December 10,2023 at 05:24:04 UTC from IEEE Xplore. Restrictions apply.